Evolution of Non-metallic Inclusions in a 303-ton Calcium-Treated Heavy Ingot

QIUYUE ZHOU, JUNTAO BA, WEI CHEN, and LIFENG ZHANG

In the current industrial trials, the modification of inclusions in a carbon-manganese steel heavy ingot by the calcium treatment was studied. The evolution of inclusions in molten steel and ingot was detected by SEM/EDS. The effect of reoxidation in tundish on inclusion composition and the precipitation of inclusion during the cooling process were calculated by computational thermodynamics. After calcium treatment, the inclusions in the molten steel were modified into liquid inclusions and a small amount of CaS was formed. Due to the serious reoxidation of the molten steel in the tundish, inclusions were only transformed into semi-solid inclusions with a composition of 60.4 pct Al_2O_3–25.3 pct CaO–7.2 pct SiO_2–7.1 pct MgO. By improving the sealing of the tundish, the inclusions in molten steel at the tundish were found to be pure liquid inclusions with the composition of 29.0 pct Al_2O_3–42.8 pct CaO–8.6 pct SiO_2–11.1 pct MgO–5.6 pct CaS–2.9 pct MnS when the reoxidation of molten steel in tundish was avoided. Thermodynamic calculation results were in agreement with the actual detected composition. The calcium treatment modified the inclusions into liquid inclusions and prevented the generation of large clusters in heavy steel ingots. The average diameter of the inclusions increased from 3.4 at the tundish to 6.17 μm at the bottom of the ingot. The heterogeneous sulfide was precipitated with the $MgO \cdot Al_2O_3$ spinel inclusions as the core. The aspect ratio of the sulfides was about 1.6, which indicated that the formation of the large MnS inclusion was avoided. Both pure solid Al_2O_3 inclusions and semi-solid inclusions aggregated in the ingot to form large inclusions, resulting in ultrasonic flaw detection defects. It is recommended to control the inclusions in heavy ingots to be pure liquid inclusions using the calcium treatment, but the reoxidation should be avoided to ensure the effective calcium treatment.

I. INTRODUCTION

CALCIUM treatment has been widely used to modify solid Al_2O_3 inclusions to liquid calcium aluminates[1] in molten steel to improve the castability of steel continuous casting. Solid Al_2O_3 inclusions tend to aggregate to form large clusters[2–4] and are easily attached to the wall of the submerged entry nozzle to generate clogging.[5] Liquid

QIUYUE ZHOU is with the School of Metallurgical and Ecological Engineering, University of Science and Technology Beijing, Beijing 100083, P.R. China. JUNTAO BA is with the College of Materials Science and Engineering, Yanshan University, Qinhuangdao 066004, P.R. China. WEI CHEN is with the School of Mechanical Engineering, Yanshan University, Qinhuangdao City, 066004 Hebei, P.R. China. Contact e-mail: weichen@ysu.edu.cn LIFENG ZHANG is with the School of Mechanical and Materials Engineering, North China University of Technology, Beijing 100144, P.R. China. Contact e-mail: zhanglifeng@ncut.edu.cn

CaO–Al_2O_3 inclusions are wetted by the molten steel[6] so that they are difficult to collide and aggregate together. Hence, it is important to modify inclusions in heavy steel ingots into liquid ones using calcium treatment. Holappa[7] and Janke[8] proposed a model to calculate the "liquid window" of Fe–O–Ca–Al–S inclusions. The sulfur in the steel should be well controlled to avoid the formation of CaS[9] that generated the clogging either. The ratio between the total calcium (T.Ca) and the total sulfur (T.S) in the steel had an influence on the mass fraction of CaO, Al_2O_3, and CaS in inclusions.[10] The content of CaO decreased with the increase of the ratio between T.S and the total oxygen (T.O) in the steel.[11,12] Liu et al.[13] found that inclusions in pipeline steel were transferred from CaO–CaS to Al_2O_3–CaO–CaS and Al_2O_3–CaO ones due to the reoxidation of the molten steel. Wang et al.[14] calculated the precise addition of calcium to the steel and established a neural network model to predict calcium yield during steel calcium treatment.

Heavy ingots can be as big as over 300 tons. Compared to the 10 to 20 minutes solidification time of the typical continuous casting process, it took approximately 3300 minute for a heavy 303-ton ingot

to be fully solidified. The long solidification time of heavy ingots generated serious sulfur segregation at grain boundaries[15] so the precipitation and growth of MnS particles occurred[16,17] and the MnS particles had a long time to grow into a millimeter size. The 16Mn steel was Al-killed and the original inclusions were Al_2O_3 inclusions. The long solidification time also allowed the collision and aggregation of oxide Al_2O_3 inclusions into millimeter-scale clusters. Figure 1(a) shows the ultrasonic flaw detection of the forged steel plate without calcium treatment. Spheres represented single defects and squares represented clustered porous defects that were marked if over five > 2 mm defects were detected within a 50 mm detection distance. Six 3–6 mm cluster defects were detected 25–60 mm beneath the surface of the steel plate and twenty-six single defects with a 7.6 mm average diameter including a 14 mm maximum one were detected 100 to 200 mm beneath the surface of the steel plate. The steel plate was rejected due to oversized inclusions. As shown in Figure 1(b), a 752 μm inclusion in a rejected roller forged from a 74-ton ingot was detected in a cluster shape, formed by the aggregation of solid Al_2O_3-based inclusions with a composition of 75.0 pct Al_2O_3–21.3 pct CaO–3.7 pctSiO_2. Both the oversize MnS particles and oxide inclusions led to the rejection of the steel product forged from heavy ingots. Due to the high production cost of heavy ingots, it is important to establish a stable and reliable calcium treatment scheme during the refining of the molten steel to modify solid Al_2O_3-based oxide inclusions into liquid ones and the subsequent occurrence of collision and aggregation of solid inclusions in the molten steel during cooling and solidification can be successfully restrained.

Extensive studies were performed to investigate the evolution of inclusions in Ca-treated steel during the refining and continuous casting process.[18–20] Additionally, the binding affinity between calcium and sulfur is stronger than that between manganese and sulfur for the reaction between calcium and alumina-based inclusions in steel, causing CaS particles to form preferentially during the solidification of the molten steel containing a specific amount of calcium and the precipitation of MnS to be delayed.[21–26] Perez et al.[27] concluded that the precipitation of MnS was weakened if the sulfur content was lower than 20 ppm and the ratio of T.Ca to T.S was in the range of 2 to 5. Due to the large cross-section of heavy steel ingots, the solidification process of the ingot was very different from that of continuous casting. However, dissecting an ingot to investigate the distribution of inclusions is a time-consuming and labor-intensive process, especially for heavy ingots, which is too
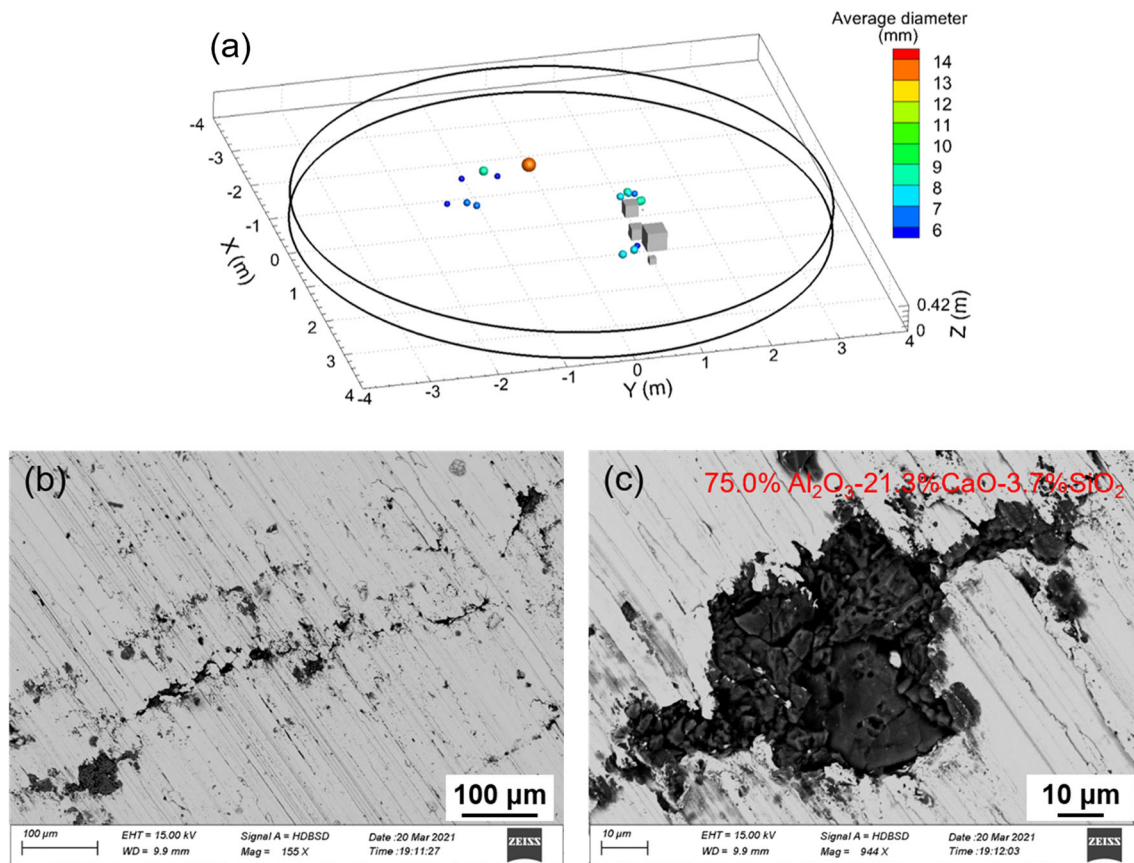

Fig. 1—Oversize inclusions in rejected forged products of heavy ingots, (a) Oversize inclusions in a rejected steel plate forged from a 303-ton ingot, (b) a 752 μm inclusion in a rejected roller forged from a 74-ton ingot, and (c) the inclusion of 75.0 pct Al_2O_3–21.3 pct CaO–3.7 pct SiO_2 at the left corner of (b).

costly. Few studies[28–30] were performed on the evolution of inclusions during the pouring and solidification process of heavy steel ingots and the evolution of inclusions in Ca-treated large steel ingots as well.

In the current study, industrial trials for the modification of Al_2O_3-based inclusions using calcium treatment during the refining of a 303-ton carbon-manganese steel ingot were carried out. The effect of reoxidation on calcium treatment was discussed, and the distribution of inclusions at the top and bottom of the ingot was analyzed. The evolution of inclusion composition was verified by thermodynamic calculation. By comparing the flaw detection defects of forged steel plates under different conditions, the optimal composition of inclusions in heavy ingots was proposed, which can guide the effective application of calcium treatment in heavy ingots.

II. SAMPLING OF INDUSTRIAL TRIALS AND ANALYSIS METHODS

In the current industrial trials, a 303-ton 16Mn steel ingot was produced by vacuum casting. The schematic diagram of the vacuum casting process is shown in Figure 2. The 303-ton heavy ingot was cast with 3 heats of the molten steel. The total vacuum casting time was 55 minute. The composition of the molten steel of different heats in tundish is shown in Table I. Since the carbon was prone to positive segregation at the top of the heavy ingot, the content of carbon in the molten steel gradually decreased from the first heat to the third heat.[31] The round tundish was placed above the vacuum tank and no mold powder was added to the surface of the molten steel in the tundish. The molten steel flowed into the ingot mold as tiny droplets when
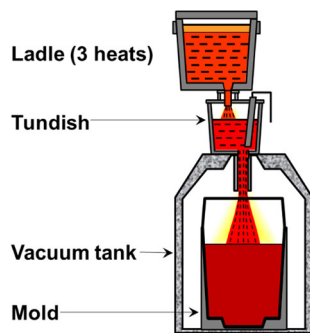
Fig. 2—Schematic diagram of vacuum casting of a 303 t steel ingot.

the degree of vacuum was less than 0.5 torr, which reduced macrosegregation and improved the cleanliness of steel.

The production route was "Electric Arc Furnace (EAF) → Ladle Furnace (LF) → Vacuum Degassing (VD) → Tundish → Vacuum Ingot Casting." Calcium treatment was carried out by inserting calcium iron cored wire with a calcium content of 42.3 pct into molten steel after the break of vacuum in VD refining. The target addition content of the calcium was 20 ppm. The molten steel samples were taken in the production of two calcium-treated ingots. The sampling process is summarized in Figure 3. Steel samples were taken after the break of vacuum, after calcium treatment in VD refining, and in tundish. The molten steel samples were taken using a stainless steel bracket sampler and then were quenched in the water immediately. The total oxygen, sulfur, and carbon contents of the steel were measured using a LECO analyzer to evaluate the effect of calcium treatment on the cleanliness of the steel. The content of Ca and Mn was measured using inductively coupled plasma mass spectrometry (ICP-MS). The evolution of inclusions in the molten steel during the VD refining process and the casting process was detected using an automatic SEM–EDS scanning system after samples were smoothed and polished. The extra high tension was 15 kV and the working distance was 8.9 mm. The number, morphology, composition, and size of inclusions in the molten steel with a diameter larger than 1 μm were analyzed. The number density and area fraction of inclusions are defined as the following two equations.

$$ND = \frac{n_{inclusion}}{A_{total}} \quad [1]$$

where ND is the number density of inclusions, #/mm²; $n_{inclusion}$ is the number of detected inclusions on the scanning area, #; A_{total} is the scanning area, mm².

$$AF = \frac{A_{inclusion}}{A_{total}} \quad [2]$$

where AF is the area fraction of inclusions, ppm; $A_{inclusion}$ is the total area of the detected inclusions, μm².

In the first calcium treatment experiment, reoxidation of molten steel was serious due to the suction of molten steel in the tundish, which offset the effect of calcium treatment. The sealing of tundish was improved and the reoxidation of molten steel in tundish was reduced by replacing the tundish cover and filling argon gas before casting. The bottom and top of the ingot with slight reoxidation were sampled every 1/3 of the

Table I. Chemical Composition of the Molten Steel in Tundish

	wt pct								ppm				
Heat	C	Si	Mn	Al	Cr	Ni	Mo	Nb	P	S	Ca	T.O	T.N
1	0.20	0.26	1.22	0.008	0.19	0.29	0.04	0.017	< 50	2.8	12	43	59
2	0.17	0.26	1.21	0.008	0.19	0.29	0.05	0.017	< 50	3.7	14	38	46
3	0.14	0.26	1.16	0.008	0.18	0.28	0.03	0.016	< 50	4.7	15	27	42

cross-sectional radius, as shown in Figure 4(a). The number, composition, morphology, and size distribution of oxide and sulfide inclusions at the bottom and top of the 303-ton ingot were analyzed to investigate the evolution of inclusions during solidification. The inclusions with a diameter larger than 2 μm in the ingot were analyzed, and the detection area of each sample was greater than 50 mm^2. Furthermore, the thermodynamic calculation of precipitation of inclusions during the solidification and cooling process of molten steel was performed using the software FactSage 7.1 with the FToxid, FactPS, and FTmisc database. Due to the small temperature gradient in the ingot during solidification, the equilibrium calculation was used in the thermodynamic calculation, where complete diffusion in the liquid phase and solid phase was considered. The range of temperature was set from 1600 °C to 1000 °C, and the cooling step was set as 10 K.

The ingot was finally forged into a steel plate. The forged steel plate was roughly ground to a surface roughness of less than Ra 6.3. Then ultrasonic flaw detection was used to detect defects larger than 2 mm in the entire steel plate as shown in Figure 4(b). The flaw detection results of the no calcium treatment, calcium treatment with severe reoxidation in the tundish, and calcium treatment with slight reoxidation in the tundish were compared.
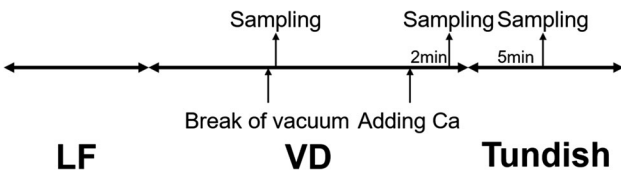
III. EFFECT OF REOXIDATION OF MOLTEN STEEL ON CALCIUM TREATMENT

Figure 5 shows the evolution of the element content in molten steel during the calcium treatment process. The T.O content decreased from 35.9 to 22.9 ppm, the T.N content decreased from 43.4 to 34.0 ppm, and the Ca content increased from 3 to 23 ppm after the addition of the calcium. However, the T.O content increased to 42.8 ppm, the T.N content increased to 59.3 ppm, and the Ca content decreased to 12 ppm in the tundish due to the serious reoxidation of the molten steel. In addition, slight reoxidation in the tundish resulted in an increase in T.O content from 23.5 to 27.5 ppm, an increase in T.N content from 34.4 to 41.9 ppm, and a decrease in Ca content from 21 to 15 ppm.

Fig. 3—Sampling locations during the production.

Fig. 5—Evolution of the element content in molten steel during the calcium treatment process.
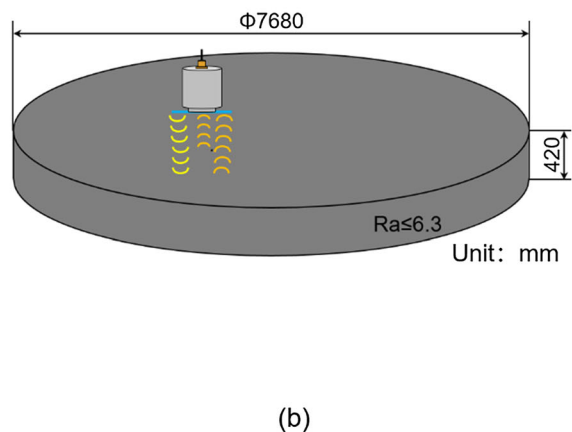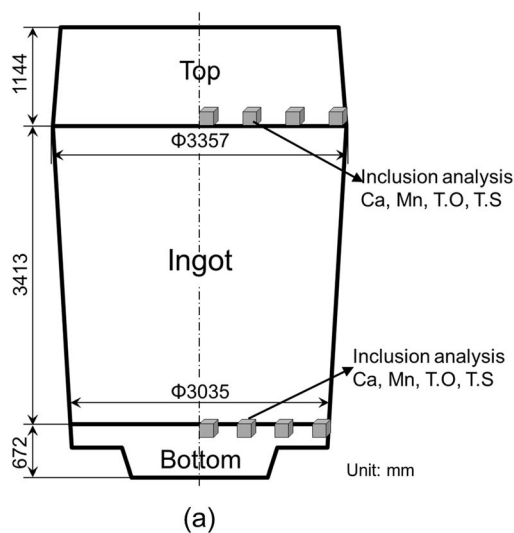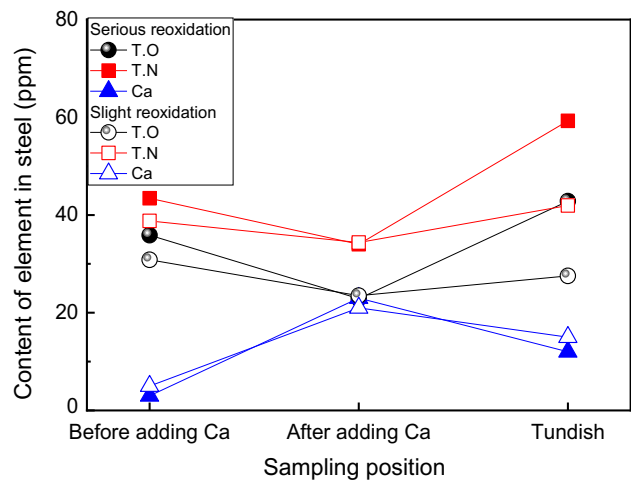

Fig. 4—Schematic diagram of the ingot sampling (*a*) and ultrasonic flaw detection of the forged steel plate (*b*).

Figure 6 shows the evolution of inclusions in molten steel with serious reoxidation in tundish. The inclusions were classified and projected onto the ternary phase diagram, and the liquidus lines of inclusions at 1673 and 1873 K were calculated by FactSage 7.1. The average composition of inclusions before calcium treatment was 61.9 pct Al_2O_3–26.8 pct CaO–4.4 pct SiO_2–6.9 pct MgO in Figure 6(a). After calcium treatment, as shown in Figure 6(b), the average composition of inclusions in the steel was 20.9 pct Al_2O_3–14.5 pct CaO–27.7 pct MgO–36.9 pct CaS. The CaS particles were formed in the molten steel in advance. The number of inclusions in molten steel was relatively reduced after the calcium treatment. As shown in Figure 6(c), the composition of inclusions in molten steel in tundish was 60.4 pct Al_2O_3–25.3 pct CaO–7.2 pct SiO_2–7.1 pct MgO. It can be seen that the CaS in inclusions was transformed into CaO, and part of the inclusions became solid inclusions.

Figure 7 shows the evolution of inclusions in molten steel with slight reoxidation in tundish. As shown in Figure 7(a), the average composition of inclusions before calcium treatment was 64.8 pct Al_2O_3–22.0 pct CaO–5.8 pct SiO_2–5.4 pct MgO–0.3 pct CaS–1.7 pct MnS. Most of the large inclusions were liquid inclusions, which originated from the slag entrainment. After calcium treatment, the average composition of
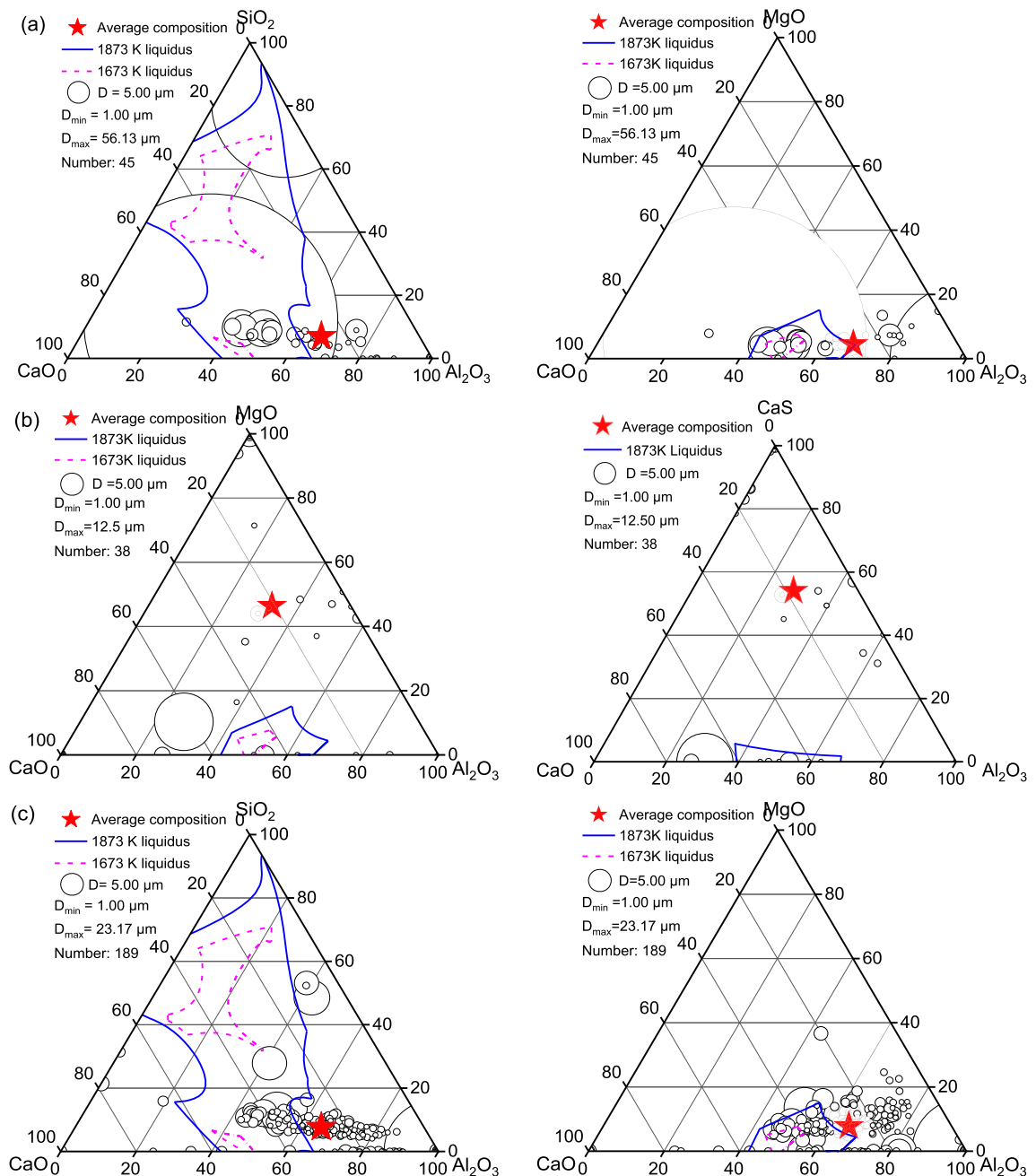

Fig. 6—Evolution of inclusions in molten steel with serious reoxidation in the tundish, (*a*) before calcium treatment, (*b*) after calcium treatment, and (*c*) tundish.
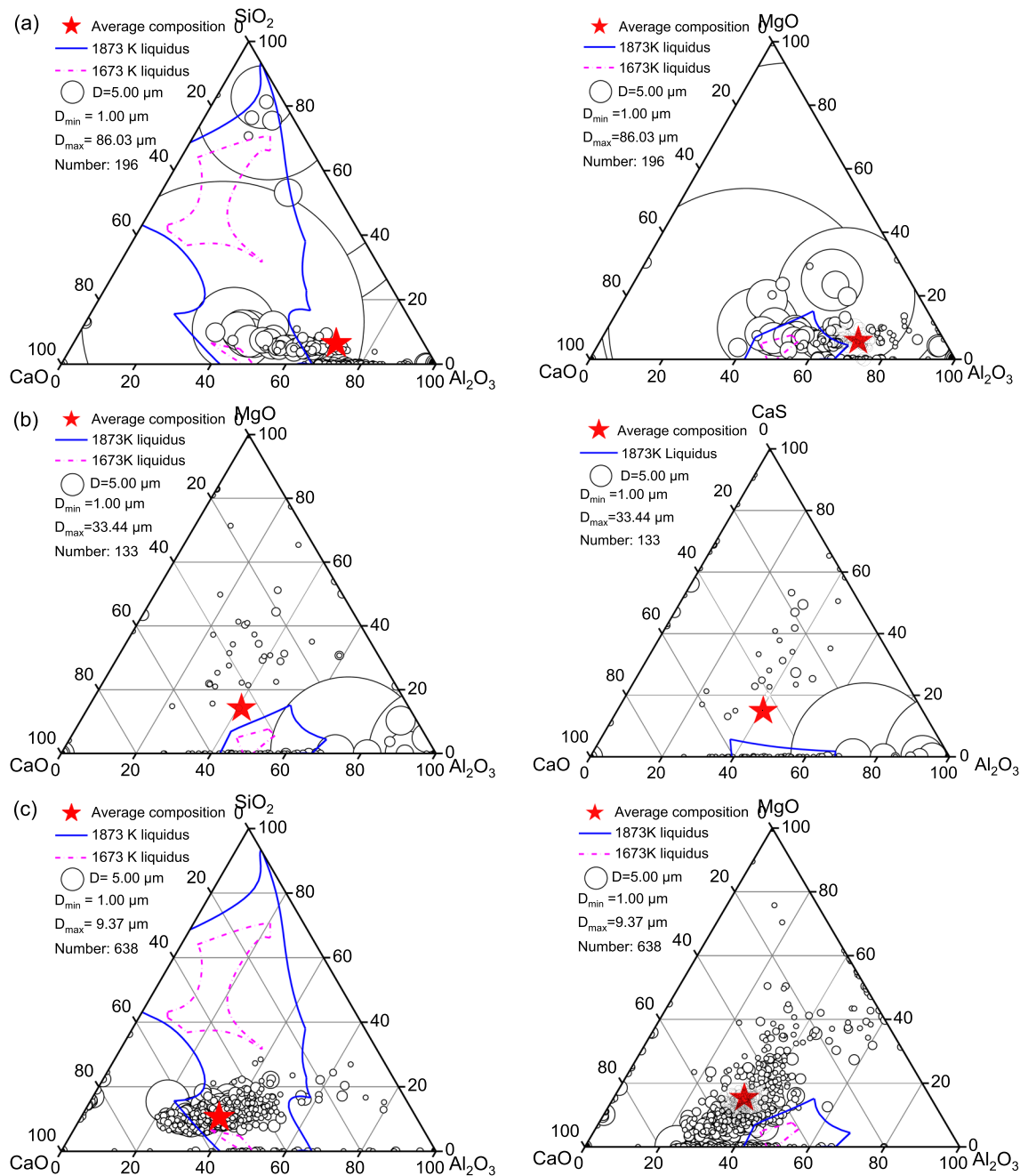
Fig. 7—Evolution of inclusions in molten steel with slight reoxidation in the tundish, (*a*) before calcium treatment, (*b*) after calcium treatment, and (*c*) tundish.

inclusions in the steel was 31.5 pct Al_2O_3–37.2 pct CaO–6.6 pct SiO_2–12.1 pct MgO–12.6 pct CaS, as shown in Figure 7(b). Since the binding ability of Ca and S was stronger than that of Mn, CaS particles with a high melting point were formed in the molten steel in advance. The number of inclusions in molten steel was reduced after calcium treatment. As shown in Figure 7(c), The composition of inclusions in molten steel in tundish was 29.0 pct Al_2O_3–42.8 pct CaO–8.6 pct SiO_2–11.1 pct MgO–5.6 pct CaS–2.9 pct MnS. Due to

the slight reoxidation of the molten steel in the tundish, The CaS in inclusions was transformed into CaO partly, and the inclusions were still liquid.

The element mapping of typical inclusions before and after calcium treatment is shown in Figure 8. A small amount of $MgO\cdot Al_2O_3$ spinel was precipitated at the edge of CaO–Al_2O_3–SiO_2 inclusion before calcium treatment as shown in Figure 8(a). The typical morphology of inclusions after calcium treatment is shown in Figure 8(b). The small size liquid inclusions were
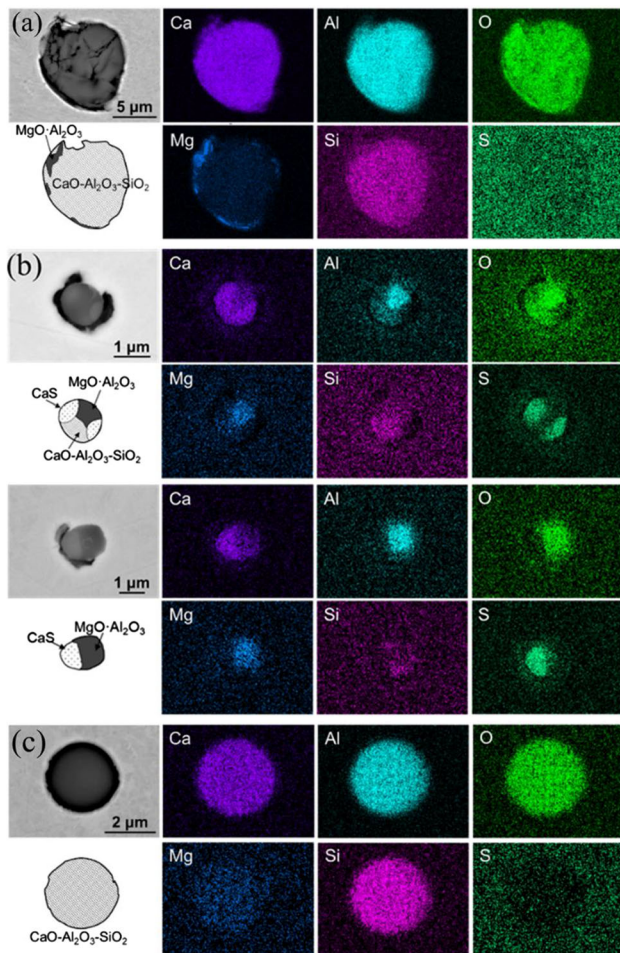
Fig. 8—Element mapping of typical inclusions in molten steel, (a) before calcium treatment, (b) after calcium treatment, and (c) tundish.

Fig. 9—Evolution of inclusion composition in molten steel during the calcium treatment.

spherical. A triple-phased morphology of CaS and MgO·Al₂O₃ spinel adhering to CaO–Al₂O₃–SiO₂ was observed. After the reoxidation of the molten steel in the tundish, the CaS in inclusions was transferred to CaO and the single-phased CaO–Al₂O₃–SiO₂ inclusions. The reoxidation of molten steel in tundish was slight and most of the inclusions were still liquid inclusions, as shown in Figure 8(c).

Figure 9 shows the evolution of inclusion composition in molten steel during the calcium treatment with different reoxidation conditions in tundish. For the serious reoxidation cases, the calcium content in the steel after calcium treatment was 23 ppm. The MgO content increased from 6.9 to 28.5 pct. The CaS content increased to 38.6 pct. The CaO content decreased from 26.8 to 12.8 pct, and the Al_2O_3 content decreased from 61.9 to 20.1 pct. After the serious reoxidation in the tundish, the average composition of inclusions was 60.4 pct Al_2O_3–25.3 pct CaO–7.2 pct SiO_2–7.1 pct MgO, which was similar to that before calcium treatment, meaning that the effect of the calcium treatment was offset by the reoxidation. For the slight reoxidation
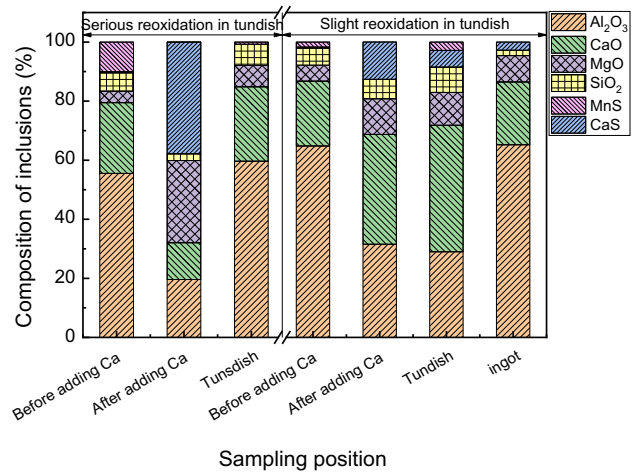
cases, the CaO content in inclusions increased from 22.0 to 37.2 pct, the CaS content increased from 0.3 to 12.6 pct, the MgO content increased from 5.4 to 12.1 pct, and the Al_2O_3 content decreased from 64.8 to 31.5 pct after calcium treatment. After a slight reoxidation of the tundish, the CaS in the inclusions was converted to CaO. The CaO content increased to 42.8 pct, while the CaS content and the Al_2O_3 content decreased to 5.6 and 29.0 pct, respectively. The inclusions were still liquid.

The comparison of the number density, area fraction, maximum diameter, and average diameter of inclusions larger than 1 μm inclusions before and after calcium treatment is shown in Figure 10. In the case of serious reoxidation in the tundish, the number density, area fraction, maximum diameter, and average diameter of inclusions decreased first and then increased from before calcium treatment to the tundish. The area fraction of inclusions after calcium treatment was less than 80 ppm and the number density was less than 4.5 #/mm². The decrease in inclusions was due to the floating and removal of inclusions caused by fluid flow. However, the number density increased from 2.33 to 15.10 #/mm², the area fraction increased from 8.99 to 74.11 ppm, the maximum diameter increased from 12.51 to 23.17 μm, and the average diameter increased from 2.05 to 2.11 μm due to the serious reoxidation in tundish. When the degree of reoxidation in the tundish was reduced, the number density increased from 4.40 to 26.52 #/mm², the area fraction increased from 68.21 to 120.81 ppm, the maximum diameter decreased from 33.44 to 9.37 μm, and the average diameter decreased from 2.03 reduced to 1.95 μm. Compared with liquid inclusions, solid inclusions with a larger contact angle were much easier to be removed from the molten steel.[32,33] The number density and area fraction of inclusions were larger in the case of slight reoxidation, and the inclusions were small in size and were liquid inclusions.

Figure 11 shows the thermodynamic calculation of the effect of reoxidation on the composition of inclusions in molten steel calculated by the FactSage 7.1 software. When the molten steel in tundish was slightly
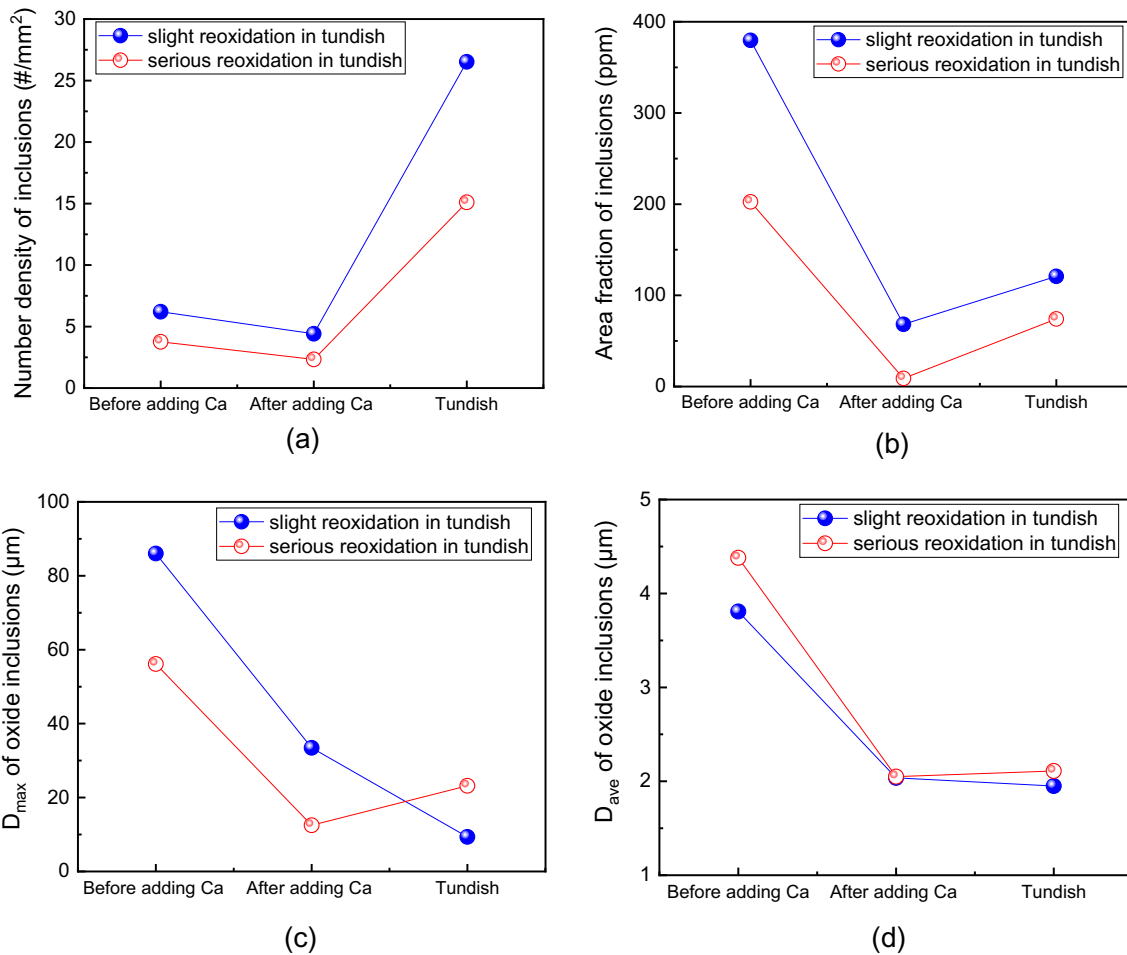
Fig. 10—Comparison of inclusion number density (*a*), area fraction (*b*), maximum diameter (*c*), and average diameter (*d*) before and after calcium treatment.
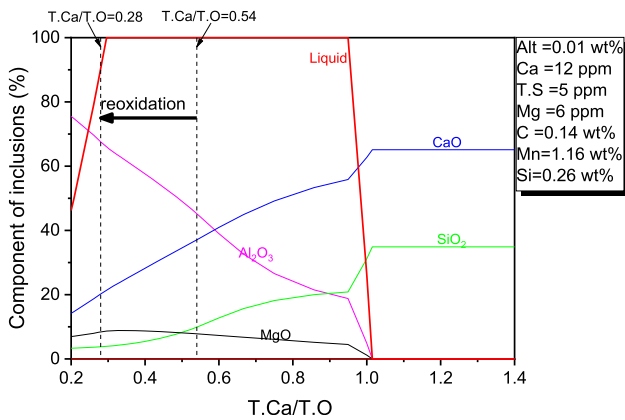

Fig. 11—Thermodynamic calculation of the effect of reoxidation on inclusion composition.

reoxidized to seriously reoxidized, the ratio between the T.Ca and T.O decreased from 0.54 to 0.28. The theoretical composition of inclusions transformed from 44.6 Al_2O_3–37.5 pct CaO–10.1 pct SiO_2–7.8 pct MgO to 67.8 pct Al_2O_3–20.3 pct CaO–3.7 pct SiO_2–8.3 pct MgO. The ratio of the liquid phase in inclusions decreased

from 100 to 90.4 pct. The thermodynamic calculation results were in good agreement with the variation of the actual inclusion composition.

IV. DISTRIBUTION OF INCLUSIONS AT THE BOTTOM AND TOP OF THE 303-TON INGOT

The composition of the steel at the bottom and top of the ingot is shown in Figure 12. At the bottom of the ingot, the maximum calcium content was at the radial center, which was 18 ppm. The calcium content at the top of the ingot was below 1 ppm. For the first heat, the carbon content was reduced from 0.20 to 0.16 pct during the vacuum casting. The carbon content at the radial center of the bottom of the ingot was 0.18 pct, the carbon content at the radial center of the top of the ingot was 0.29 pct, and the carbon content at the top of the ingot gradually decreased from the center to the edge. The sulfur content in the radial center at the bottom of the ingot was 4.61 ppm, and the sulfur content in the radial center at the top of the ingot was 13.02 ppm. From the radial center to the edge, the T.O content decreased from 34.2 to 8.4 ppm at the bottom of
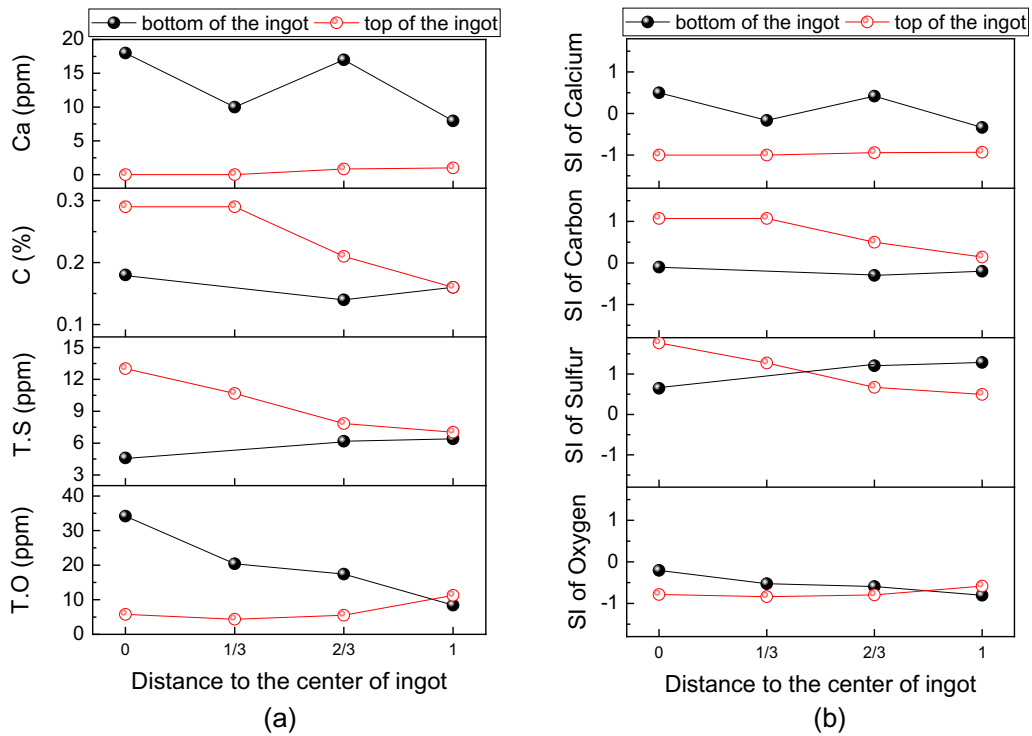
Fig. 12—Element composition (*a*) and segregation index (*b*) of the steel at the bottom and top of the ingot.

the ingot, and the T.O content increased from 5.8 to 11.3 ppm at the top of the ingot conversely. In addition, the Mn content in the steel at the bottom and top of the ingot was 1.17 pct and 1.35 pct, respectively. The segregation index ($SI = (C_{mix} - C_0)/C_0$) of different elements is shown in Figure 12(b), the negative segregation of oxygen and calcium in the ingot was caused by the floating of oxide inclusions. Carbon presented negative segregation at the bottom of the ingot and positive segregation at the top of the ingot. The maximum segregation index of carbon was 1.07 at the radial center of the top of the ingot. Sulfur presented positive segregation in the ingot. The maximum segregation index of sulfur was 1.77 at the radial center of the top of the ingot.

The ternary phase diagram of inclusions at different positions at the bottom of the ingot is shown in Figure 13. The average composition of inclusions was 65.3 pct Al_2O_3–21.3 pct CaO–1.8 pct SiO_2–8.9 pct MgO–2.7 pct CaS. Compared with the inclusions in the tundish, the Al_2O_3 content increased, while the CaO and SiO_2 content decreased, and the inclusions were transformed into solid inclusions. The MgO·Al_2O_3 spinel inclusions were precipitated during the solidification of the molten steel. The average composition of inclusions larger than 20 μm was 52.1 pctAl_2O_3–29.9 pctCaO–9.2 pctMgO–8.8 pctSiO_2, which originated from the slag entrainment in the ladle. The slag entrainment inclusions were concentrated at the bottom of the ingot at a 2/3 radius from the radial center. Inclusions were mainly small MgO·Al_2O_3 spinel and large slag entrainment inclusions due to the fast solidification and cooling rate at the edge of the ingot.

The typical morphology of the inclusions at the bottom of the ingot is shown in Figure 14. The gray part of the large inclusion in Figure 14(a) was the liquid CaO–Al_2O_3 inclusion, and a large amount of black MgO·Al_2O_3 spinel inclusions was formed inside and around the inclusion. In addition, the CaS was found to precipitate at the edge. The typical morphology of small inclusions is shown in Figure 14(b). Light gray sulfides with a composition of 79.9 pct CaS–20.1 pct MnS were precipitated on the CaO–Al_2O_3 inclusions, and then MgO·Al_2O_3 spinel inclusions were precipitated.

Figure 15 compares the number density, area fraction, maximum diameter, and average diameter of inclusions larger than 2 μm at the bottom of the ingot and the molten steel in the tundish. The number density of inclusions larger than 2 μm in the molten steel in tundish was 11.07 #/mm^2. The number density of inclusions larger than 2 μm at the bottom of the ingot was smaller than that of the molten steel in the tundish and gradually decreased from 8.77 to 0.52 #/mm^2 from the center to the edge along the radial direction. This may be caused by the floating and the collision of the inclusions during the solidification of the ingot. The area fraction and average diameter of inclusions at different positions at the bottom of the ingot were larger than the 140.3 ppm area fraction and 3.4 μm average diameter of the molten steel in the tundish, respectively. From the molten steel in the tundish to the center of the bottom of the ingot, the average diameter of the inclusions increased from 3.4 to 6.17 μm. The liquid inclusions were less likely to aggregate to form large clusters during the solidification of the ingot. The maximum value of the area fraction, maximum diameter, and average
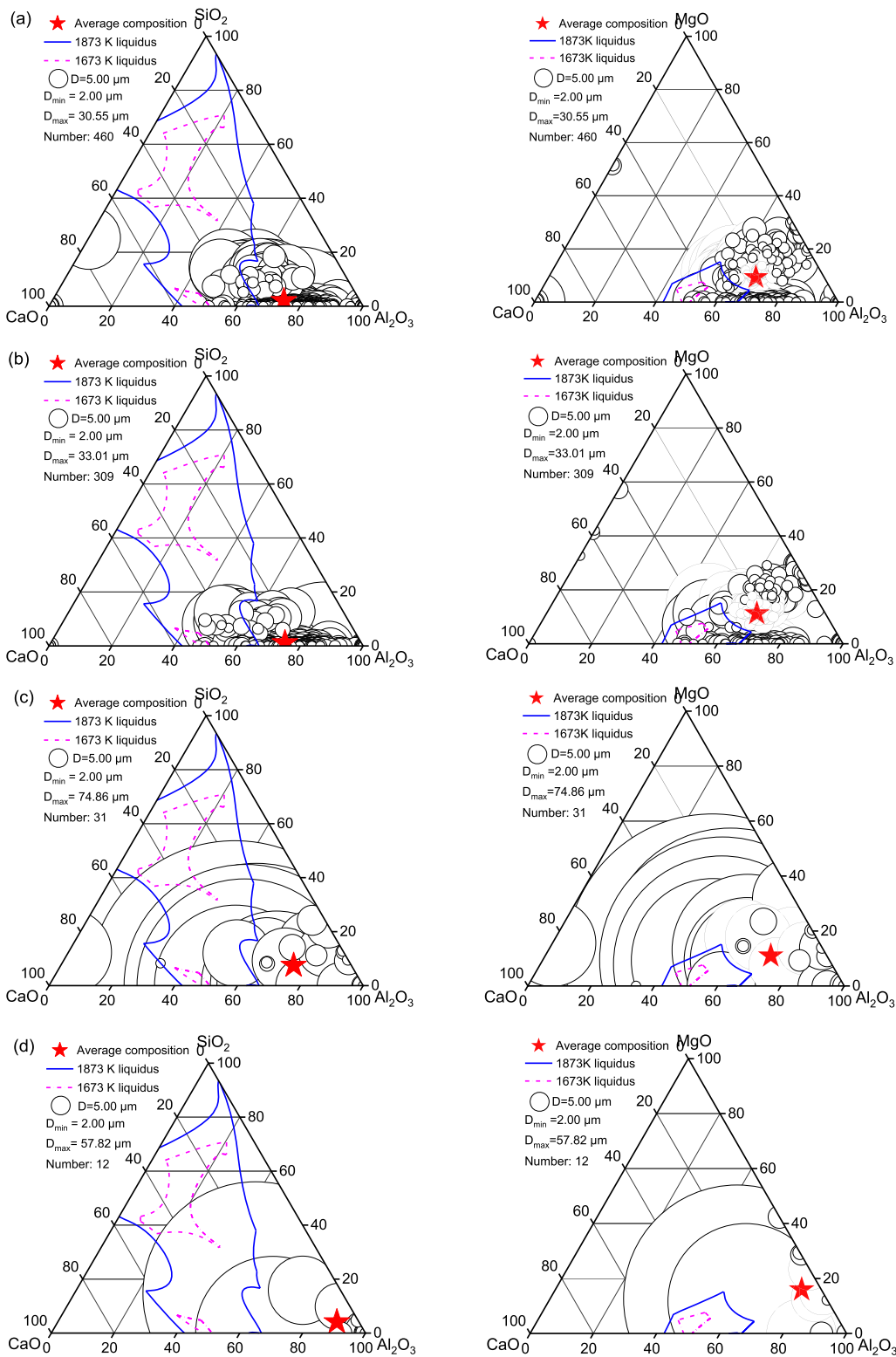
Fig. 13—Ternary phase diagram of inclusions at different positions of the bottom of the ingot, (*a*) at the radial center, (*b*) at the 1/3 radius from the radial center, (*c*) at the 2/3 radius from the radial center, and (*d*) at the radial edge.

diameter of inclusions at the bottom of the ingot was 371.2 ppm, 74.9, and 21.1 μm, respectively, and appeared at the 2/3 radius from the radial center of the ingot. During the floating process of inclusions, they were captured by crystal rain and settled to the bottom,

causing the accumulation of inclusions at the bottom of the ingot. Large inclusions were more likely to gather at the bottom. In the radial direction, the inclusion population was found to be highest in the center part of the ingot.[34,35]
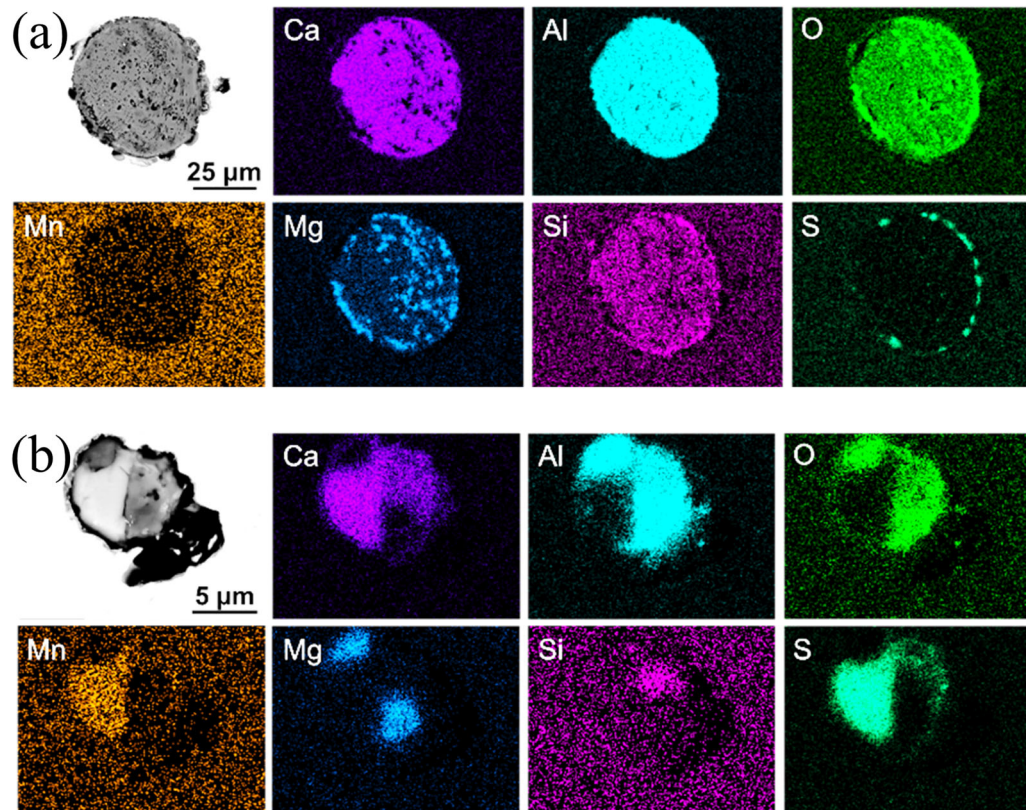
Fig. 14—Typical morphology of inclusions at the bottom of the ingot, (*a*) large inclusion and (*b*) small inclusion.

Since the solidification time of the current ingot was long enough, the inclusions were floated at the top of the ingot. Inclusions at the top of the ingot were mainly sulfides. As shown in Figure 16(a), the diameter of the homogeneous nucleated MnS was less than 30 μm, and the typical morphology was spherical or polyhedral. The typical morphology of the heterogeneous nucleated sulfide and the element mapping results are shown in Figures 16(b) and (c), respectively. The MnS took the black MgO·Al$_2$O$_3$ spinel as the core and precipitated in the radial center. However, the light gray sulfide of 71.8 pct CaS–28.2 pct MnS was precipitated with the MgO·Al$_2$O$_3$ spinel core at the edge of the ingot.

Figure 17 shows the number density, area fraction, maximum diameter, average diameter, and aspect ratio of sulfide inclusions at the top of the ingot. The number density of pure MnS inclusions was less than 1.0 #/mm^2. The maximum number density was 0.79 #/mm^2 and appeared at the 1/3 radius from the radial center of the ingot. The number density of heterogeneous nucleated sulfides was less than 0.3 #/mm^2. As shown in Figure 17(b), there were more pure MnS inclusions near the center of the ingot and more heterogeneous nucleated sulfides in the edge. Similar to the distribution of inclusions at the bottom of the ingot, the oxide inclusions, *i.e.*, the heterogeneous nucleation core, were most abundant at the 2/3 radius from the radial center of the ingot. The maximum diameter of the MnS inclusion was decreased from 34.2 to 4.37 μm along the

center to the edge of the ingot, while the maximum diameter of heterogeneous nucleated sulfides was increased from 20.67 to 37.54 μm. In addition, the aspect ratio of the inclusions was about 1.6, which indicated that calcium treatment had a good effect on the modification of large MnS inclusions.

From the molten steel in the tundish to the bottom of the ingot, the average composition changed from 48.0 Al$_2$O$_3$–34.4 pct CaO–7.5 pct SiO$_2$–9.8 pct MgO–0.3 pct CaS to 65.3 pct Al$_2$O$_3$–21.3 pct CaO–1.8 pct SiO$_2$–8.9 pct MgO–2.7 pct CaS. The content of Al$_2$O$_3$ in the inclusion was increased and the content of CaO was decreased. According to the results of the thermodynamic analysis, the transition of inclusion at the radial center of the bottom of the ingot is shown in Figure 18(a). The liquid inclusions transformed into solid CaAl$_4$O$_7$ and CaAl$_2$O$_4$ as the temperature decreased. The CaS inclusion was precipitated at 1341.1 °C, but in small quantities. The transition of inclusion at the radial edge of the bottom of the ingot is shown in Figure 18(b). The CaS inclusion precipitated on the liquid calcium aluminate at 1431.7 °C. The amount of the precipitated CaS increased with the decrease in the temperature. The precipitation of sulfide at the center of the top of the ingot during the cooling process is shown in Figure 18(c). The MnS took the MgO·Al$_2$O$_3$ as the core and precipitated at 1121.6 °C. As shown in Figure 18(d), the CaS was precipitated at 1121.8 °C first
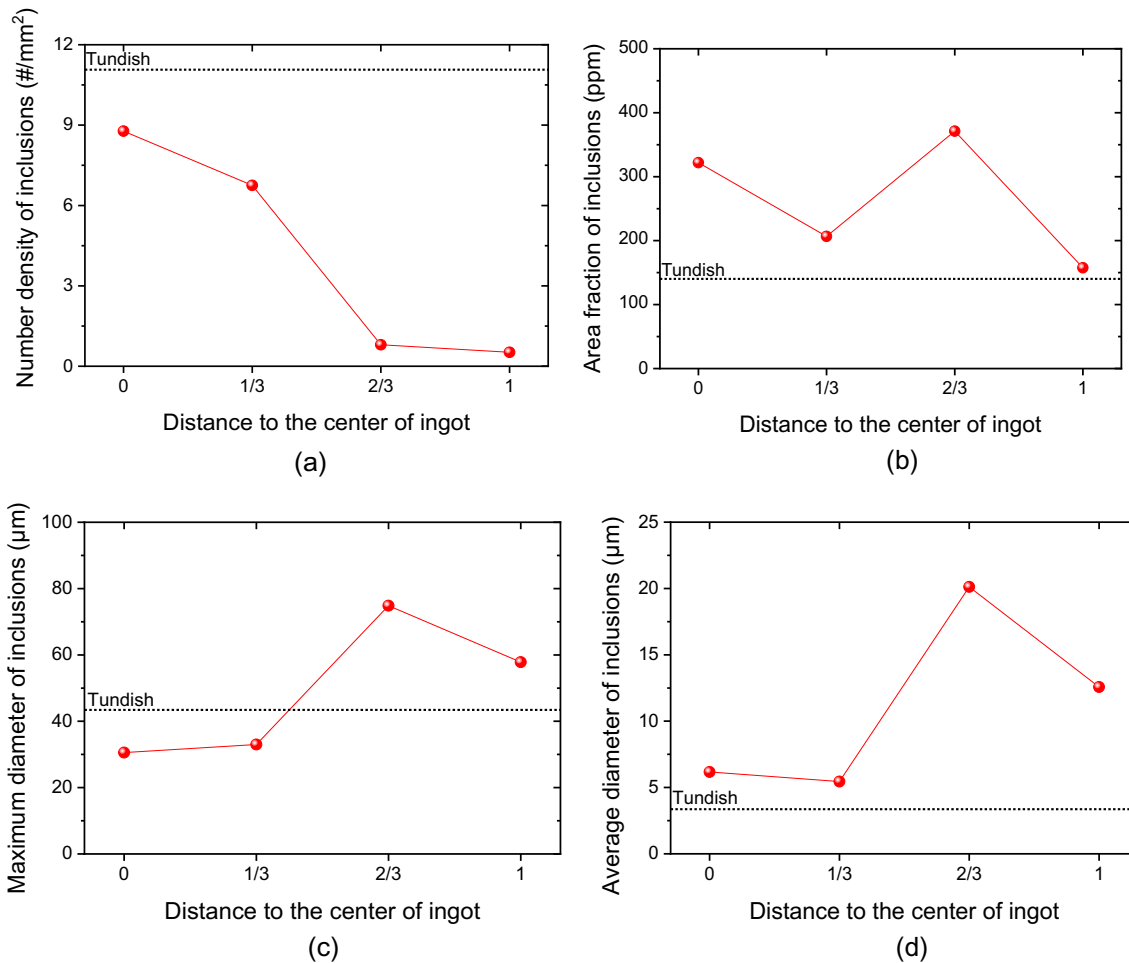
Fig. 15—Comparison of inclusions larger than 2 μm at the bottom of the ingot and the molten steel in the tundish, (*a*) number density, (*b*) area fraction, (*c*) maximum diameter, and (*d*) average diameter.

and then the MnS was precipitated at 1065.7 °C with the 1 ppm Ca content in the steel, which was consistent with the observed actual inclusions.

V. OPTIMUM COMPOSITION OF INCLUSIONS IN HEAVY INGOTS

Figure 19 shows the morphology of different types of inclusions after aggregation. The solid Al_2O_3 inclusion was mainly large clusters with diameters larger than 0.5 mm. The composition of the semi-solid calcium aluminate inclusion was 60.4 pct Al_2O_3–25.3 pct CaO–7.2 pct SiO_2–7.1 pct MgO, which was in a string-like shape and larger than 0.2 mm in diameter. The composition of the liquid calcium aluminate inclusion was 29.0 pct Al_2O_3–42.8 pct CaO–8.6 pct SiO_2–11.1 pct MgO–5.6 pct CaS–2.9 pct MnS. The morphology of the liquid calcium aluminate inclusion was spherical. The inclusions were mutually exclusive and the maximum diameter was about 80 μm. Pure solid Al_2O_3 inclusions aggregated most seriously, semi-solid inclusions also aggregated in molten steel,

and liquid inclusions repelled each other in molten steel. Since the solidification time of large steel ingots over 100 tons was as long as over 24 h, the collision and aggregation of solid inclusions were so serious to generate millimeter-scale big inclusions in the steel ingot. In conclusion, the calcium treatment modified inclusions into pure liquid inclusions and prevented the generation of the clustered inclusions in the ingot.

Figure 20 shows the effect of the calcium treatment and reoxidation on the distribution of defects. The original inclusions in the tube sheet without calcium treatment were solid Al_2O_3, and the aggregation of inclusions resulted in excessive defects in the scrapped tube sheet. The number of defects with equivalent diameters of 2 to 4, 4 to 6, 6 to 8, and 8 to 10 mm was 5, 3, 24, and 22, respectively. The inclusions in the tube sheet with severe reoxidation in the tundish were semi-solid CaO–Al_2O_3. Although the inclusions were not completely converted to a liquid state due to the reoxidation, the large-scale defects were still much smaller than those without calcium treatment. The inclusions in the calcium-treated tube sheet were liquid
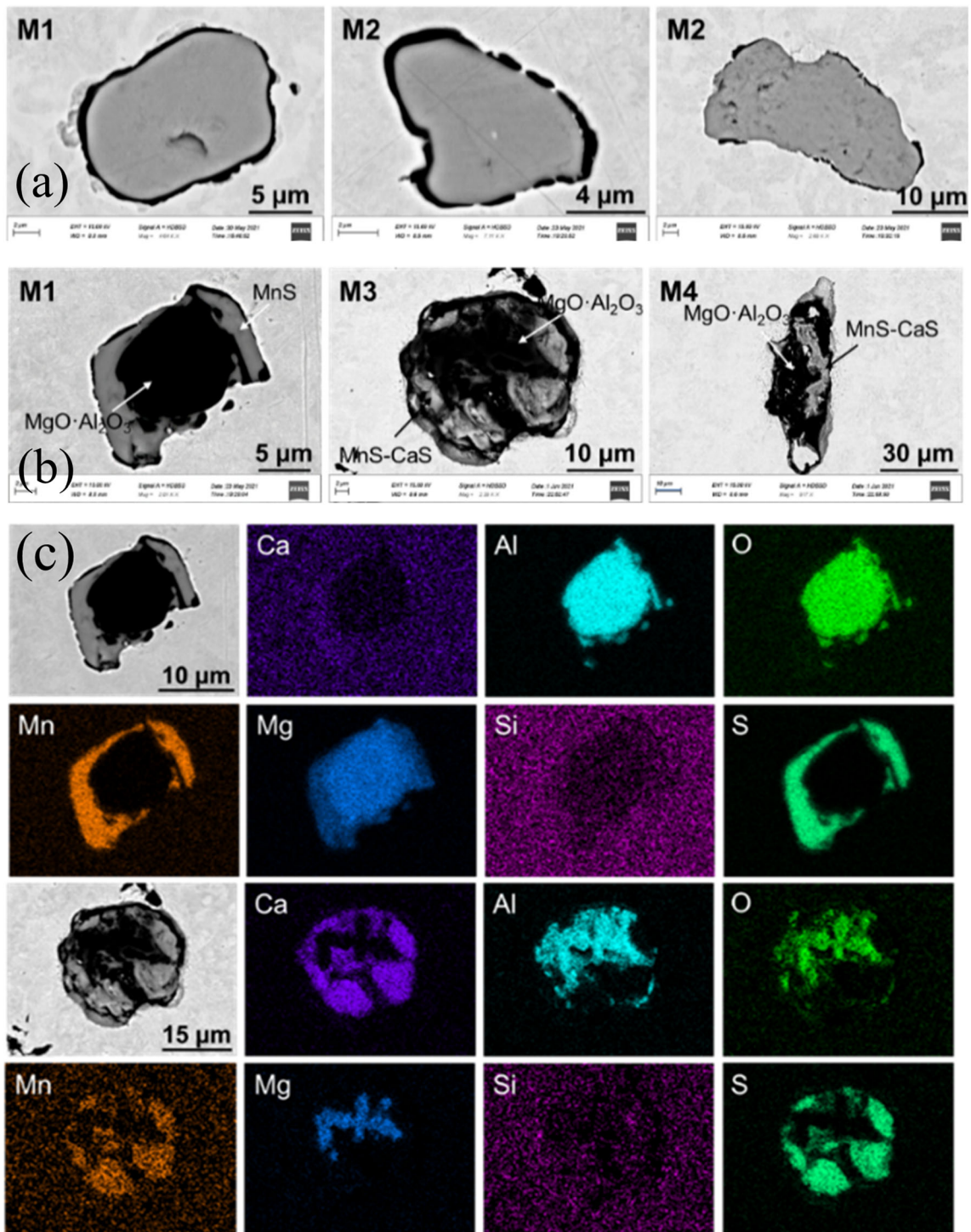
Fig. 16—Typical morphology and element mapping of inclusions at the top of the ingot, (*a*) typical homogeneous nucleated MnS, (*b*) typical heterogeneous nucleated sulfide, and (*c*) element mapping of typical heterogeneous nucleated sulfides.

$CaO-Al_2O_3$. The quality of the tube sheet was significantly better than that of the calcium-treated tube sheet with reoxidation in tundish and the no calcium-treated tube sheet. The number of detected defects was reduced to 7 and all of them were small-size defects with an equivalent diameter of 2 to 4 mm after the calcium treatment. The ultrasonic flaw detection results of the tube sheet indicated that it was more appropriate to control the inclusions in heavy ingot to be pure liquid inclusions.
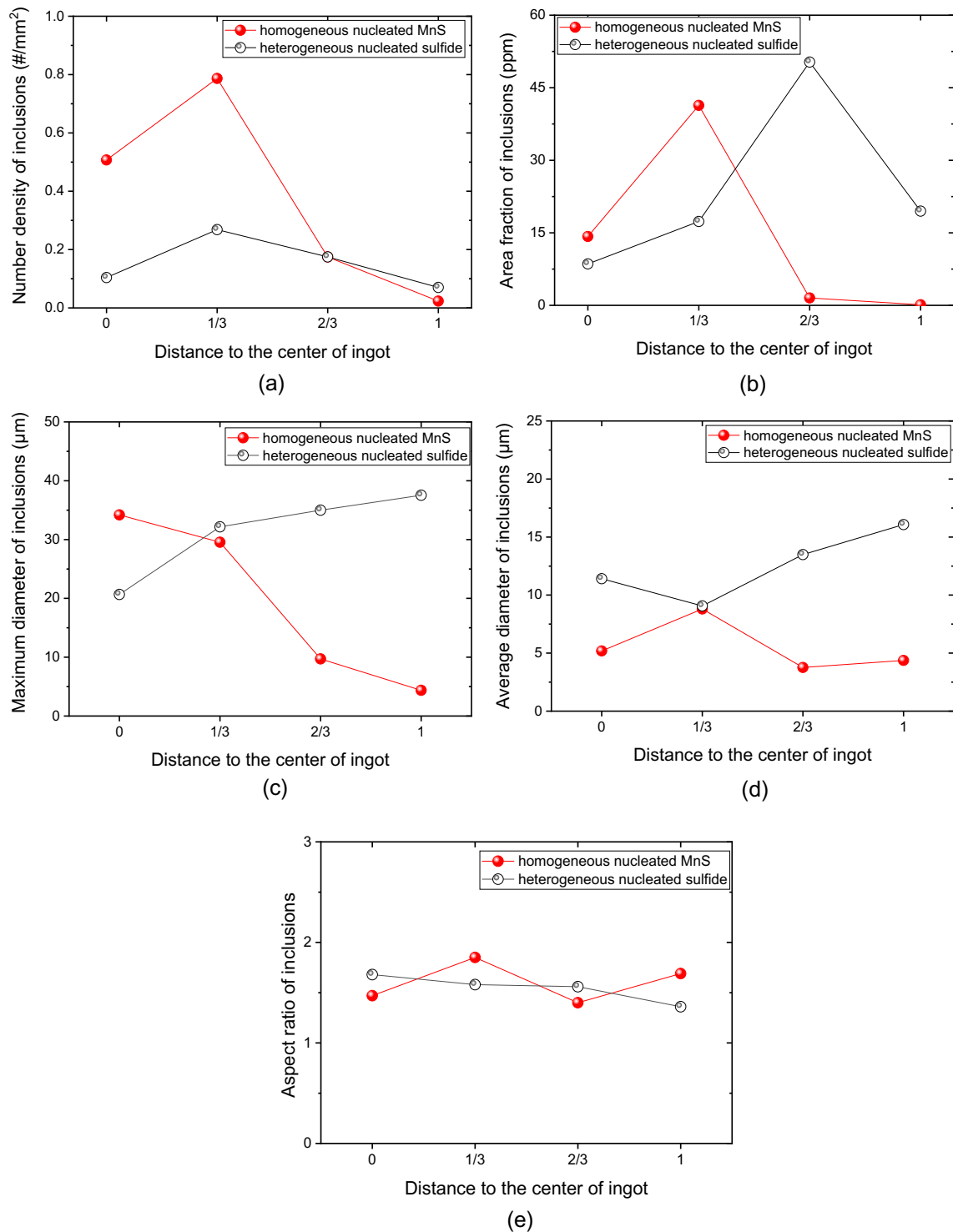
Fig. 17—Number density (*a*), area fraction (*b*), maximum diameter (*c*), average diameter (*d*), and aspect ratio (*e*) of sulfide inclusions at the top of the ingot.

Figure 21 summarizes the evolution of non-metallic inclusions with different conditions in heavy 303-ton ingots. In the case of no calcium treatment shown in Figure 21(a), the inclusions in the molten steel during the VD refining process were mainly solid CaO–Al_2O_3, and the reoxidation of the molten steel in the tundish led to the transformation of the inclusions into Al_2O_3.

Finally, the large-size Al_2O_3 clusters were formed in the ingot due to the collision of solid Al_2O_3 inclusions. As shown in Figure 21(b), when the molten steel was calcium treated with severe reoxidation in the tundish, the MgO·Al_2O_3–CaS inclusions in the molten steel were transformed into string shape semi-solid CaO–Al_2O_3 inclusions in the ingot.
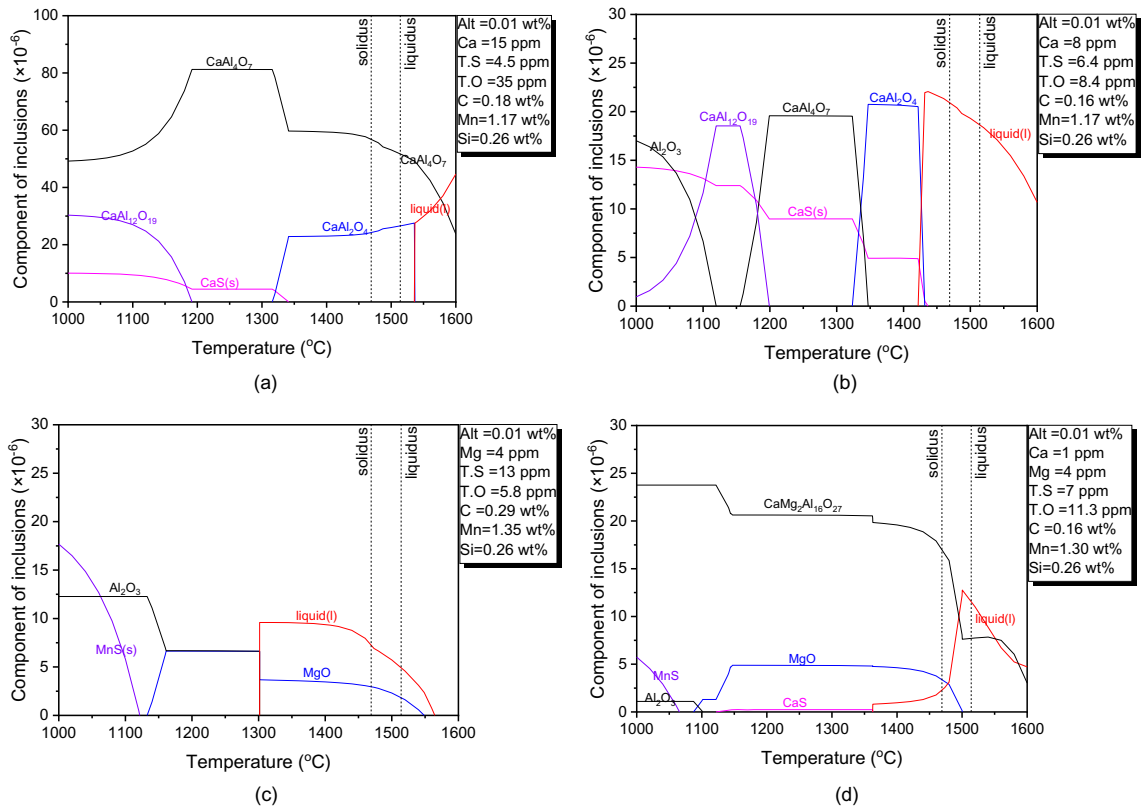
Fig. 18—Thermodynamic analysis of inclusion composition during solidification of ingot, (*a*) radial center of the bottom of the ingot, (*b*) radial edge of the bottom of the ingot, (*c*) radial center of the top of the ingot, and (*d*) radial edge of the top of the ingot.

Figure 21(c) shows the evolution of inclusions in molten steel with effective calcium treatment. The solid CaO–Al$_2$O$_3$ inclusions were transformed into liquid CaO–Al$_2$O$_3$ with a large amount of CaS after the calcium treatment. A slight reoxidation of molten steel in the tundish resulted in the conversion of a small amount of CaS to CaO, while the inclusions were still liquid CaO–Al$_2$O$_3$. During the solidification process of the ingot, the small-sized inclusions with an average diameter of 6.17 μm concentrated at the center of the bottom of the ingot, and slag entrainment inclusions larger than 50 μm concentrated at the 2/3 radius from the radial center of the ingot. The liquid oxide inclusions were fully floated and the small-sized homogeneous and heterogeneous MnS inclusions were precipitated with a 1.6 aspect ratio at the top of the ingot. The calcium treatment not only prevented the aggregation of inclusions at the bottom, but also prevented the generation of large-sized Type II MnS inclusions at the top of the ingot.

VI. CONCLUSIONS

Industrial trials were performed to study the effect of calcium treatment on the modification of inclusions in a 303-ton 16Mn steel ingot. The conclusions were summarized as follows.

(1) After calcium treatment, the inclusions in the molten steel were modified into liquid inclusions and a small amount of CaS was formed. The T.O content was found to increase from 22.9 to 42.8 ppm due to the serious reoxidation of the molten steel in the tundish, which caused the inclusions to transform into semi-solid inclusions with a composition of 60.4 pct Al$_2$O$_3$–25.3 pct CaO–7.2 pct SiO$_2$–7.1 pct MgO. When the reoxidation of molten steel in tundish was improved, the inclusions in molten steel at the tundish were found to be pure liquid inclusions with the composition of 29.0 pct Al$_2$O$_3$–42.8 pct CaO–8.6 pct SiO$_2$–11.1 pct MgO–5.6 pct CaS–2.9 pct MnS. Thermodynamic calculation results were in agreement with the actual detected composition.

(2) From the tundish to the center of the bottom of the ingot, the average diameter of the inclusions increased from 3.4 to 6.17 μm. The composition of inclusions was 67.0 pct Al$_2$O$_3$–22.0 pct CaO–9.1 pct MgO–1.9 pct SiO$_2$, and the content of Al$_2$O$_3$ in the inclusions was increased while the content of CaO was decreased. The calcium treatment modified the inclusions into liquid inclusions and prevented the generation of large clusters in heavy steel ingots. Large slag entrainment inclusions were concentrated at the bottom of the ingot at a 2/3 radius from the radial center.
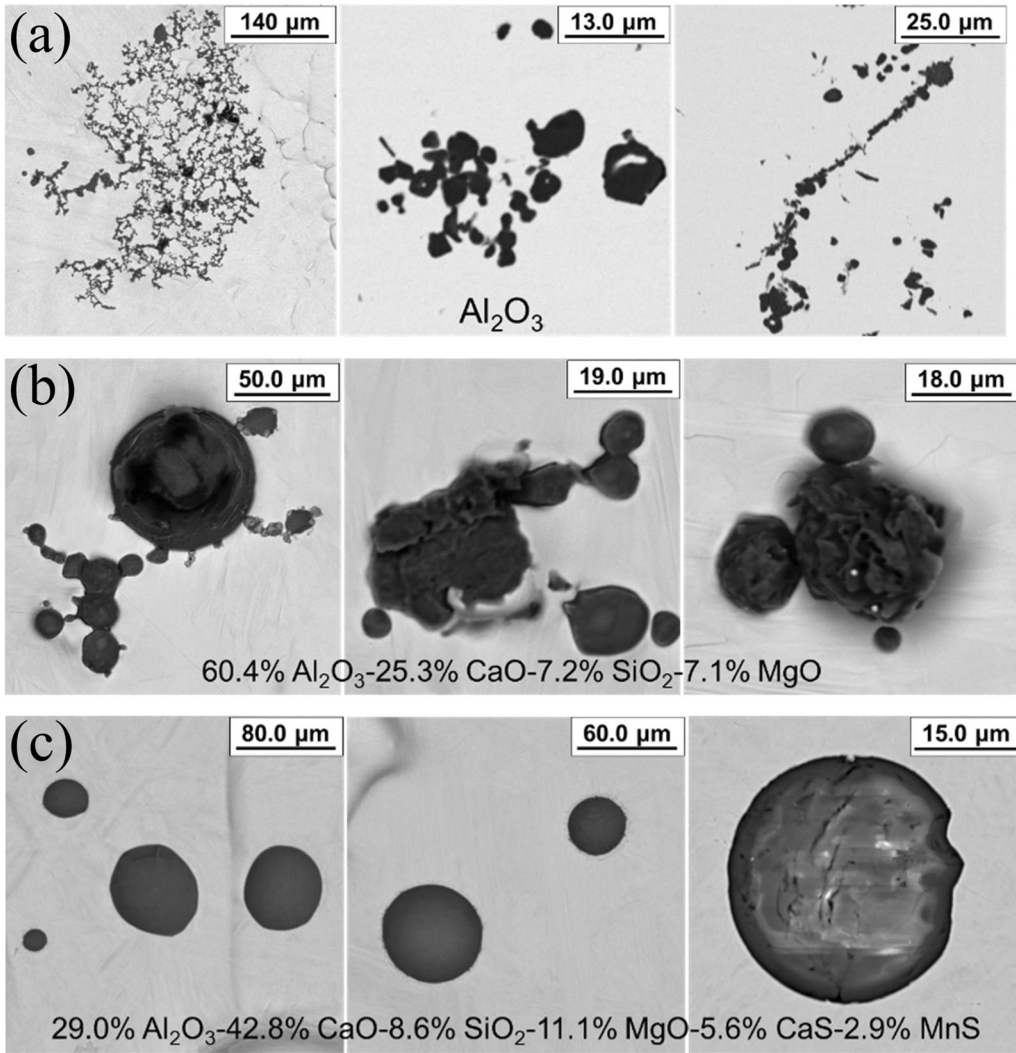
Fig. 19—Morphology of inclusions with different liquid phase fractions after aggregation, (*a*) solid inclusions, (*b*) semi-solid inclusions, and (*c*) liquid inclusions.
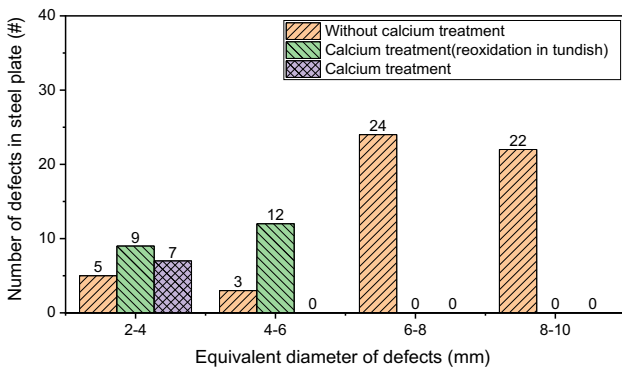

Fig. 20—Effect of the calcium treatment and reoxidation on the distribution of defects.

(3) The diameter of the homogeneous nucleated MnS at the top of the ingot was less than 30 μm, and the typical morphology was spherical or polyhedral. The heterogeneous sulfide took the $MgO \cdot Al_2O_3$ spinel as the core and then precipitated. The CaS was precipitated at 1121.8 °C first and then the MnS was precipitated at 1065.7 °C. The aspect ratio of the sulfides was about 1.6.

(4) The optimum composition of inclusions in heavy steel ingots was pure liquid inclusions. Pure solid Al_2O_3 inclusions aggregated most seriously, semi-solid inclusions also aggregated in molten steel, and liquid inclusions repelled each other in molten steel, which was consistent with the results of ultrasonic flaw detection. The calcium treatment can effectively
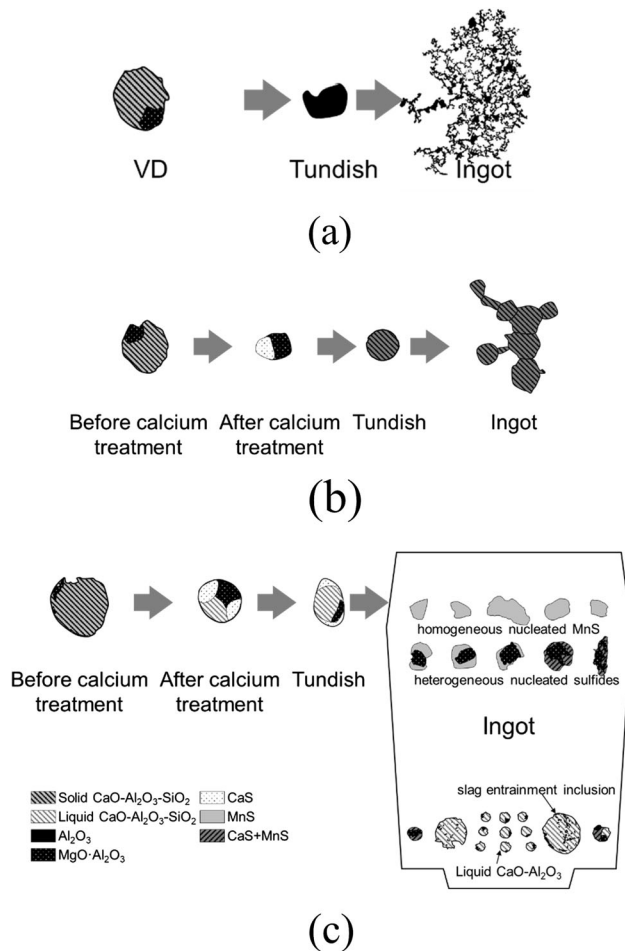
Fig. 21—Evolution diagram of non-metallic inclusions in heavy 303-ton ingots, (*a*) without calcium treatment, (*b*) calcium treatment with serious reoxidation in the tundish, and (*c*) calcium treatment with slight reoxidation in the tundish.

transform solid inclusions into liquid inclusions, but reoxidation should be avoided to ensure the effect of calcium treatment.

CONFLICT OF INTEREST

On behalf of all authors, the corresponding author states that there is no conflict of interest.

REFERENCES

1. G. Ye, P. Jönsson, and T. Lund: *ISIJ Int.*, 1996, vol. 36, pp. S105–8.
2. W.Y. Kim, G.J. Nam, and S.Y. Kim: *Metall. Mater. Trans. B.*, 2021, vol. 52B, pp. 1508–20.
3. L. Zhang: *Non-metallic Inclusions in Steels: Fundamentals*, Metallurgical Industry Press, Beijing, 2019. (**in Chinese**).
4. Y. Kang, B. Sahebkar, P.R. Scheller, K. Morita, and D. Sichen: *Metall. Mater. Trans. B*, 2011, vol. 42B, pp. 522–34.
5. Z. Deng and M. Zhu: *ISIJ Int.*, 2013, vol. 53, pp. 450–58.
6. Y. Wang and C. Liu: *Metall. Mater. Trans. B*, 2020, vol. 51B, pp. 2585–95.
7. L. Zhang: *Non-metallic Inclusions in Steels: Industrial Practice*, Metallurgical Industry Press, Beijing, 2020. (**in Chinese**).
8. N. Shinozaki, N. Echida, K. Mukai, Y. Takahashi, and Y. Tanaka: *Tetsu-to-Hagané*, 1994, vol. 80, pp. 748–53.
9. L. Holappa, M. Hämäläinen, M. Liukkonen, and M. Lind: *Ironmak. Steelmak.*, 2003, vol. 30, pp. 111–15.
10. D. Janke, M. Zhongting, and P. Valentin: *ISIJ Int.*, 2000, vol. 40, pp. 31–39.
11. Y. Wang, S. Sridhar, and M. Valdez: *Metall. Mater. Trans. B*, 2002, vol. 33B, pp. 625–32.
12. Q. Ren and L. Zhang: *Metall. Mater. Trans. B*, 2020, vol. 51B, pp. 589–600.
13. Y. Liu, L. Zhang, Y. Zhang, H. Duan, Y. Ren, and W. Yang: *Metall. Mater. Trans. B*, 2018, vol. 49B, pp. 610–26.
14. J. Xu, F. Huang, and X. Wang: *Metall. Mater. Trans. B*, 2016, vol. 47B, pp. 1217–27.
15. L. Zhang, Y. Liu, Y. Zhang, W. Yang, and W. Chen: *Metall. Mater. Trans. B*, 2018, vol. 49B, pp. 1841–59.
16. W. Wang, L. Zhang, Y. Ren, Y. Luo, X. Sun, and W. Yang: *Metall. Mater. Trans. B*, 2022, vol. 53B, pp. 1–7.
17. C. Maidorn and D. Blind: *Nucl. Eng. Des.*, 1985, vol. 84, pp. 285–96.
18. U. Yoshiyuki, Y. Hidetoshi, M. Shozo, and K. Hiroyuki: *Tetsu-to-Hagane*, 1989, vol. 75, p. 5010508.
19. H.S. Kim, H.G. Lee, and W.G. Jung: *ISIJ Int.*, 2000, vol. 40, pp. S82-86.
20. W. Wang, L. Zhang, Y. Luo, Y. Ren and X. Sun: *Ironmak. Steelmak.*, 2021, pp. 1–12.
21. W. Yang, L. Zhang, X. Wang, Y. Ren, X. Liu, and Q. Shan: *ISIJ Int.*, 2013, vol. 53, pp. 1401–10.
22. W. Yang, C. Guo, C. Li, and L. Zhang: *Metall. Mater. Trans. B*, 2017, vol. 48B, pp. 2267–73.
23. H. Wu, P. Lu, F. Yue, L. Zhou, W. Chen, and D. You: *J. Univ. Sci. Technol. Beijing*, 2014, vol. 36, pp. 230–34.
24. L. Luyckx, J.R. Bell, A. McLean, and M. Korchynsky: *Metall. Trans.*, 1970, vol. 1, pp. 3341–50.
25. L. Dong and X. Liu: *Iron Steel*, 1987, vol. 22, pp. 51–55.
26. T. Ikeda, N. Fujino, and H. Ichihashi: *Tetsu-to-Hagané*, 1980, vol. 66, pp. 2040–49.
27. T.E. Perez, H. Quintanilla and E. Rey: in *Corrosion 98*, 1998.
28. O. Haida, T. Emi, K. Sanbongi, T. Shiraishi, and A. Fujiwara: *Tetsu-to-Hagane*, 1978, vol. 64, pp. 1538–47.
29. L. Zhang and B.G. Thomas: *Metall. Mater. Trans. B*, 2006, vol. 37B, pp. 733–61.
30. D. Cai, F. Ren, H. Ge, H.-S. Kim, J. Li, and J. Li: *Metall. Mater. Trans. A*, 2019, vol. 50A, pp. 1323–32.
31. V. Doub, A. Romashkin, and A. Malginov: *Metallurgist*, 2013, vol. 57, pp. 487–504.
32. H. Ling, L. Zhang, and H. Li: *Metall. Mater. Trans. B*, 2016, vol. 47B, pp. 2991–3012.
33. W. Liu, S. Yang, and J. Li: *Chin. J. Eng.*, 2021, vol. 43, p. 1647.
34. J. Liu, Y. Yang, C. Zhuang, X. Cui, and Y. Li: *J. Univ. Sci. Technol. Beijing*, 2011, vol. 31, pp. 179–84.
35. N. Tripathi and D. Sichen: *Scand. J. Metall.*, 2004, vol. 33, pp. 362–69.